POLITECNICO
MILANO 1863

SCUOLA DI INGEGNERIA INDUSTRIALE
E DELL'INFORMAZIONE

Executive Summary of the Thesis

HERA mission trajectory safety assessment through on-board failure detection

Laurea Magistrale in Space Engineering - Ingegneria Spaziale

Author: Pietro Califano

Advisor: Prof. Michéle Roberta Lavagna

Co-advisor: Jesús Gil-Fernández

Academic year: 2022-2023

---

1. Introduction

Near-Earth Asteroids, with a perihelion distance estimated to be less than 1.3 AU, are scientifically relevant targets for deep space exploration missions. Binary asteroid systems in particular, such as (65803) Dydimos and its secondary Dimorphos, offer valuable insights into the intricate interaction between two celestial bodies, encompassing their complex gravitational dynamics, the formation and evolution of such systems, and their interaction with the Solar system environment.

1.1. Hera Mission context

The AIDA collaboration by NASA and ESA consists of two interrelated yet independent missions, DART and Hera [2], aiming at demonstrating Kinetic Impactor technology for altering the trajectory of potentially hazardous asteroids. The Hera mission is entirely dedicated to in-depth system characterization, studying the impact caused by DART. Stringent requirements are imposed on Operations, Guidance, Navigation, and Control (GNC) capabilities, as well as close approach trajectories. The close-proximity operations span approximately 22 weeks across three nominal mission phases and an experimental phase. A progressive enhancement in on-board autonomy coupled with a reduction in the distance from the asteroid is foreseen throughout these phases, up to the full autonomy during the EXP. In particular, on-board guidance algorithms will be enabled: a manoeuvre correction term $\delta\mathbf{v}$ will be computed based on the estimated state at the manoeuvre times as provided by the Navigation. Additionally, thrusters failures are particularly critical in low gravity environments and can lead to unsafe trajectories. It is thus advisable to augment the GNC functionalities with Failure Detection and Isolation (FDI) algorithms, capable of detecting any safety issue and suggesting collision avoidance manoeuvres (CAM) actions during autonomous operations.

Navigation architecture The Hera spacecraft is equipped with two cameras and an altimeter, serving for on-board navigation. The IP algorithms extract the centroid coordinates by processing acquired image, then fed to an EKF. These include *Maximum correlation with Lambertian Sphere* and *Centre of Brightness*, designed for relative navigation on Didymos and Dimorphos, respectively.

1.2. Research Objectives

In past interplanetary missions to small bodies, safety concerns were addressed by relying on Ground Flight Dynamics and planning. This involves ensuring safety through conservative margins, validated by covariance and Monte Carlo analyses of different mission scenarios and uncertainties [3]. The trajectory re-design process is performed iteratively during the close proximity operations phase, with adjustments based on the most recent batch of received data after the data cut-off point.
While the current paradigm has proven effective, an autonomous spacecraft capable of detecting collision risks could significantly reduce the time and costs associated with early characterizations, while enhancing the robustness in highly uncertain systems. The Hera mission is pioneering the ability to assess trajectory safety "on-line". The present work aims at assessing possible methodologies to autonomously conduct this evaluation from a navigation standpoint.

2. On-board Collision assessment methodologies

Three methods were developed to assess the safety of the trajectory processing the available observables. As output, a flag suggesting a CAM is raised whenever a potential collision risk is identified.

2.1. Measurement Only Collision Risk Estimator (MOCRE)

It operates without relying on a model of the spacecraft motion, only requiring range and line-of-sight information to the primary attractor (Didymos). The conjunction assessment problem is formulated based on the prediction of the distance at closest approach (DCA) variable, modeled as Gaussian distribution. Therefore, mean estimate $\hat{r}_{CA}$ and variance $\sigma^2_{\hat{r}_{CA}}$ have to be estimated. An analytical solution given the spacecraft current state appears as the sole viable option to achieve fast enough computation. The primary issue that prevents the estimation of $\hat{r}_{CA}$ by propagation is the long integration time as well as its dependency on the spacecraft position. Therefore, the assumption of Keplerian dynamics must be leveraged. Exploiting two integrals of motion, namely orbit energy and angular momentum, two version of an analytical function yielding the pericentre distance are derived. Eq.(1) maps the state vector, whereas eq.2 achieves the same result given the distance r, the radial velocity $\dot{r}$ and the true anomaly rate $\dot{\theta}$. The Unscented Transform was employed to minimize the linearization error in the uncertainty propagation.
The simplest and most conservative approach consists in the definition of a Keep-out sphere (KoS) of radius R_{KoS} the spacecraft must not cross. This was set to 1362 m, considering Dimorphos orbit, size and margin. The evaluation of the probability of the spacecraft to enter the KoS is simply defined in terms of the integral of the miss distance distribution. Finally, the CAM decision problem, is addressed by comparing the resulting probability against a threshold Pr_{max}.
The MOCRE does not allow the estimation of the entire state vector. Therefore, Least-Squares Regression with time-polynomials [5] of the measurements is employed to calculate the smoothed value of the range $r(t_{est})$, the range-rate $\dot{r}(t_{est})$ and the true-anomaly rate $\dot{\theta}$ at each estimation time t_{est}. Their variances is approximated from the RMS of the post-fit residuals, founded on the understanding that the it serves as empirical measure of the dispersion of the errors introducing the uncertainty. The estimation of $\dot{\theta}$ relies on approximating the $\Delta\theta$ through the displacement of N_θ Line of Sight (Los) corresponding to the centroid measurements over the smoothing time window, computed w.r.t. the first valid Los (fig. 1).

2.2. Parallel filter

A filter with simplified models re-processes the same measurements as the Extended Kalman filter (KF) does for the Navigation functionality. A Square-Root Unscented Schmidt KF [4] was chosen for the increased robustness the UKF guarantees. Two variants were designed: 1) a Keplerian elements filter with analytical propagator based on the solution of Kepler's problem; 2) a classical filter in Cartesian coordinates. The augmentation of the state with the gravitational parameter μ_{D1} of the main body as considered parameter was studied in an attempt to include known uncertainties in the estimation process.
Thanks to the Square Root covariance, the DCA

$$r_p(\mathbf{r},\mathbf{v}) = \frac{-\mu + \sqrt{\mu^2 + \left(r^2 v^2 - (-\mathbf{r}\cdot\mathbf{v})\right)\left(v^2 - 2\mu/r\right)}}{\left(v^2 - 2\mu/r\right)} \tag{1}$$

$$r_p(r,\dot{r},\dot{\theta}) = \frac{-\mu + \sqrt{\mu^2 + \left(r^4\dot{\theta}^2\right)\left(\dot{r}^2 + r^2\dot{\theta}^2 - 2\mu/r\right)}}{\left(\dot{r}^2 + r^2\dot{\theta}^2 - 2\mu/r\right)} \tag{2}$$

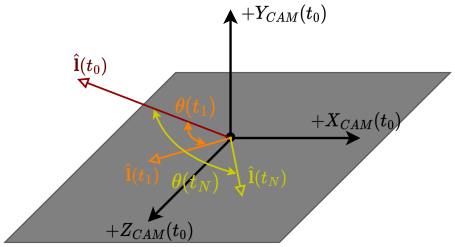

Figure 1: Representation of the line-of-sight vectors displacements with respect to the first in a window starting at time t_0.

computation can be rapidly performed starting from the available pool of sigma points. The simple relation $\hat{r}_{CA} = \hat{a}(1-\hat{e})$ is employed for the Keplerian state filter, whereas the Cartesian state one uses eq. (1).
The filters comprise the observation models predicting altimeter and IP measurements. The former predicts the altimeter measurement from the spacecraft to the surface of the target body, modeled as tri-axial ellipsoids. The latter provides the coordinates of the centre of mass for Didymos and the centre of brightness for Dimorphos. Both IP models are based on the pinhole projection model. However, a corrective shift computed through a Lambertian sphere scattering law is added to account for the Sun phase angle in the second case. The attitude quaternion of the spacecraft is assumed perfectly known from the attitude determination filter.
The design assumes a diagonal matrix with altimeter $\sigma_{Alt} = 40\,m$; whereas the centroiding covariance sub-matrix is computed through a nonlinear function of the prior estimated state. The tuning of the process noise was performed based on filter consistency evaluation, with the objective of relying only State Noise Compensation (SNC) to "cover" the errors due to modeling uncertainties and biases. Two tuning matrices are used, one for bearing-only navigation, the other for use after the altimeter activation.

Manoeuvres are accounted for adding discrete $\Delta\mathbf{v}$ and dispersion to the velocity covariance at each manoeuvring time.
The Cartesian filter differs in the motion model, which can include all the relevant perturbation terms. While the Observation Update remains unchanged, the transformation of the state to Cartesian coordinates is no longer necessary. However, numerical integration, performed with an Euler integration scheme, must be employed.

2.3. Constrained filters bank-based Wald Sequential Probability Ratio Test (SPRT)

Two constrained SRUSKF are run in parallel within the framework of binary hypothesis inferential tests. The Wald SPRT is exploited for the decision process, based on the sequentially update of the Likelihood ratio of the filters Innovations PDFs [1]. The latter ones are approximated as Gaussian distributions with mean $\boldsymbol{\varepsilon_k}$ and covariance W_k.

$$\Lambda_k = \frac{p\left(\mathbf{Y}_{1:k}|H_1\right)}{p\left(\mathbf{Y}_{1:k}|H_0\right)} \simeq \frac{N\left(\boldsymbol{\varepsilon}_{k|1:k-1,H_1}, W_{k|1:k-1,H_1}\right)}{N\left(\boldsymbol{\varepsilon}_{k|1:k-1,H_0}, W_{k|1:k-1,H_0}\right)} \tag{3}$$

In filtering terms, as the evaluation point moves farther from the mean and as the innovation covariance increases, the value entering the ratio for the i^{th} filter decreases. Hence, the constraint deriving from the hypothesis makes one of the two filters "matching" more the actual observations. Based on the targeted missed detection (md) and false alarm (fa) probabilities, the decision bounds of the test, A and B, are computed.

$$\begin{cases} \Lambda_k \geq A \;\Rightarrow\; H_0 \text{ rejected} \\ \Lambda_k \leq B \;\Rightarrow\; H_1 \text{ rejected} \end{cases} \tag{4}$$

The two hypothesis are straightforwardly defined in terms of the distance at closest approach, analytically computed under the Two body problem assumption and of the Keep-out

sphere radius.

$$\begin{aligned} H_0 &: r_{CA} = ||\mathbf{r}(t_{CA})|| \leq R_{KoS} \\ H_1 &: r_{CA} = ||\mathbf{r}(t_{CA})|| > R_{KoS} \end{aligned} \tag{5}$$

The filters process measurements as they arrive at each "current" timestep t_k, and the constraint is enforced after each update. The Sigma-Point projection is selected for the constraint enforcement as it seamlessly integrates with the implementation of the SRUSKF. It is to be noted that only one of them undergoes constraining at any time due to the complementary nature of the hypotheses. The problem of mapping the constrained states backward in time up to the current time instant t_k is identifiable as a two point boundary value problem, and specifically a targeting problem. The keplerian dynamics assumption enables the use of a Lambert's problem solver. The filters employed to construct the bank were implemented in the simplest formulation possible. They estimate the orbital state vector only, with constant measurement noise covariance, and without the addition of process noise. It was found that the on-board application presents a *fundamental* difference w.r.t. ground applications: the capability of the estimators to predict the measurements depends upon the filter state trajectory and the attitude knowledge. The immediate consequence is that if the estimated trajectory differs too much from the real one, either of the two filter stops predicting physically consistent measurements even though sensors and IP provide a valid input (fig. 2). In such cases, the sequential update of the Likelihood ratio stops before having reached a decision and a secondary detection method is activated: a counter is initiated and consecutively incremented at each timestep if the rejection consistently originates from the same filter. A tunable threshold on the elapsed time is defined and a decision is inferred based on which of the two filters, hence hypothesis, is failing. This situation becomes more frequent as the spacecraft approaches the asteroids, with the trajectory playing an increasingly crucial role in determining whether the bodies are within the altimeter beam and camera view.

From an operational standpoint, a *coupled* configuration was chosen among three alternatives: the filters bank and the test are re-initialized from the last available navigation solution at start-up, during manoeuvres and every time a decision is taken by the SPRT.

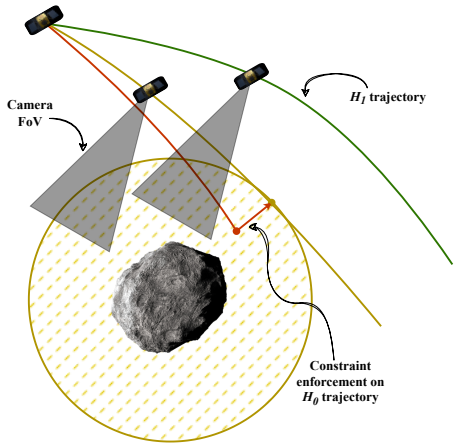

Figure 2: Two-dimensional representation of the spacecraft loosing the target body due to constraint enforcement in the Nominal EXP (safe)

3. Results and discussion

3.1. Simulation models

The Hera mission GNC simulator was used to generate the reference trajectories for this study. All the relevant perturbations acting on the spacecraft were included, namely: Didymos, Dimorphos, SRP, Sun, Earth, Mars, Non-modeled and control accelerations and internal perturbations. The measurements dataset were primarily generated using the high fidelity model (HFM), which encompasses the entire GNC hardware and software, as well as the IP algorithms. Synthetic images were generated in closed-loop from the simulation data using PANGU software. Simplified models, identical to filter ones were also employed to generate measurements in the ideal and "artificially noisy" cases.

An analysis of the dynamical environment showed that both Dimorphos and the SRP exert a significant influence in determining the spacecraft trajectory. However, the propagation errors under the Keplerian motion assumption were deemed acceptable for FDI purposes, even if not for navigation.

3.2. Simulation setup and analysis

Two scenarios were tested during the analysis:

1. **Nominal** EXP trajectory, where no colli-

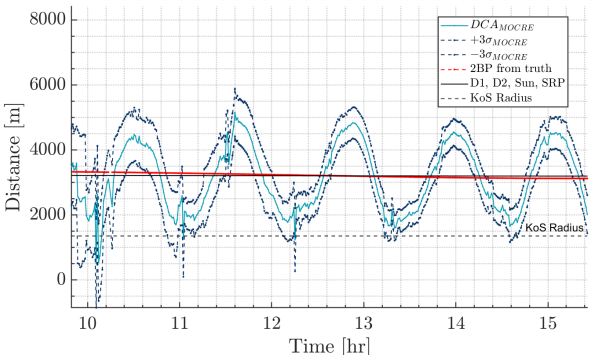

Figure 3: MOCRE closest approach distance evaluation with HFM measurements - Nominal EXP (Default tuning).

sion risk exists.

2. **Unsafe** EXP trajectory, forced toward an unsafe position using the 1^{st} manoeuvre.

MOCRE analysis The algorithm was tuned to use a first and third order polynomial for the fitting of range and displacement respectively, and a sliding time window of $1\,hr$ as default tuning. An extended window of $2\,hr$ was also tested to assess the performance improvements.
A preliminary evaluation in the nominal scenario aimed to validate the algorithm implementation while assessing the contribution of the Keplerian dynamics assumption in the prediction error. Under ideal conditions, the method exhibits minimal error, primarily linked to the assumptions and secondarily to the finite-size window of estimation. A second analysis evaluated the impact of artificially noisy measurements, bridging the gap between ideal and HFM results. The capability of the smoother to predict the DCA on average was demonstrated, but the variance approximation from the post-fit residuals determined a significant uncertainty bound the estimator cannot reduce. No false alarm was triggered in this case, while the safety issue was nearly perfectly detected in the unsafe EXP scenario. On the contrary, the nominal scenario using HFM measurements revealed major performance degradation, signalling that the additional noise and error sources invalidate the LS assumptions and renders the estimator inconsistent (fig. 3). The centroiding measurements were identified as the primary contributor to the estimation error, specifically affecting the true-anomaly rate estimate. Numerous false alarms were triggered as a consequence.
The extended window tuning achieved significant improvement in the accuracy, completely avoiding the occurrence of false alarms. However, the uncertainty bound remained large as it mainly depends upon the measurements precision. In conclusion, the Keplerian dynamics assumption is the primary factor contributing to prediction errors when measurement noise is minimal, establishing a lower bound on the achievable accuracy. The number of samples was confirmed to be the key tuning parameter of the noise reduction capability. The variance estimation proved to be excessively coarse.

Parallel filter analysis The accuracy, consistency and DCA prediction accuracy of three filter variants were evaluated for both scenarios through multiple MC analysis, initializing with 100 scattered state errors. The scattering was performed assuming an accuracy comparable with the ground orbit determination. The three variants are Keplerian state (KEP), Cartesian state (CartKEP) both in two body-dynamics and adding SRP and 3^{rd} body perturbations (CartHF). The Camera frame was preferred as it provides a clearer insight into the estimation process of the filter. The estimation errors with 3σ covariance bounds of the CartHF in the nominal scenario are shown in fig. 4. For all variants, the Z boresight errors revealed the lower observability of the distance when only the centroid is available, followed by a rapid improvement as the altimeter is incorporated. In fact, the flown trajectory lacks significant changes in parallax. The visual inspection of the estimation errors indicated that the filters are unable to converge to the "true" trajectory due to the uncorrected estimation bias. However, this feature was expected "by design". The position estimation error was bounded for most of the trajectory, with some caveats: the Keplerian state filter begins to fail as the spacecraft approaches the system; the process noise tuning is crucial in maintaining a sufficiently large covariance bound after the altimeter activation; the bore-sight range starts to lose consistency slightly before the altimeter activation, due to the covariance shrink and the estimation error not being corrected; the large necessary process noise affects the smoothness of the esti-

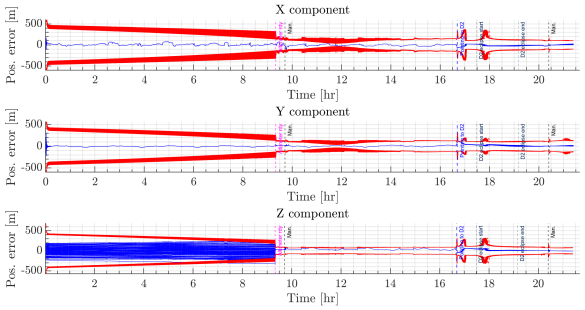

Figure 4: Cartesian HF: Position Estimation errors (blue solid) and 3σ covariance bounds (red dashed) - Nominal EXP @CAM frame.

mated trajectory. Little difference was noticed between CartKEP and CartHF, likely due to the high measurements frequency and to the SNC. The present analysis also revealed a major difference between keplerian elements and cartesian coordinates: the former filter is not able to properly "extract information" from the observables, notably as a result from the fact that none of the Keplerian elements is directly observable, At the same time, little correlation between the states builds up during propagation. Additionally, the measurement update of the keplerian filter was found to nullify the computational advantage of the analytical propagation in case of a small propagation time. As for the considered gravitational parameter, it determined excessively large covariance bounds of the velocity states, reaching values of km/s. This in turn, clearly caused the Unscented Transform to capture non-linear effects and fail, such that this design feature had to be discarded. Additional simulation results showed that the filters only slightly and slowly reduce the velocity covariance with respect to the initialization value. The DCA prediction including the considered state resulted in a continuous false alarm, while this occurred only after the second manoeuvre when the state was removed. Evidently, a conflict exists between the permissible process noise for consistent estimation and the necessity of avoiding false alarms in the detection. Finally, filter consistency was evaluated for the CartHF using the averaged NEES statistics test at 95% confidence level, effectively confirming the existence of a large systematic estimation error.
The unsafe case unveiled a second major issue of the Keplerian state space, in that the filter is not able to cope with large uncertainties in combination with eccentricity values near 1. This is understandable by noting that the structure of the motion model changes between elliptical and hyperbolic orbits, and ultimately renders the keplerian state filter impractical. Little difference in the estimation performance was noted w.r.t. the nominal scenario, with the exception of a more pronounced offset in the error. However, despite the fact that the filter managed to track the trajectory, SNC fell short of ensuring consistency of the position states maintaining the nominal tuning. The DCA prediction remained accurate enough to correctly identify the safety issue.

Constrained filters bank-based Wald SPRT The evaluation of the filter bank concept focused exclusively on filters utilizing Cartesian coordinates, specifically employing the 2-body problem motion model. In fact, enhanced accuracy is not a strict requirement given that the SPRT is driven by the performance of one filter *relative* to its complementary counterpart. The target md and fa probabilities were set equal to $\bar{P}_{fa} = 1 \times 10^{-4}$, $\bar{P}_{md} = 1 \times 10^{-10}$, aiming at minimizing the likelihood of a missed detection in the unsafe scenario. The threshold of the decision counter was set equal to 6 and 288 measurement updates, respectively for bearing-only and "altimeter-in-the-loop" navigation. The secondary mode threshold was fixed to 1 hr. A random scattering of the initial errors was performed for each sample run.
In the nominal scenario tests, the effect of the scattering was primarily determinant in the decision process during bearing-only navigation, due to the larger position errors. All the sample runs attained the same decisions after the altimeter activation. Systematic decision errors were experienced in the nominal case, plausibly caused by measurements outliers being incorporated. However, this could not be verified within the scope of the present study. The selection of tuning parameters were found to have a significant influence on the performance, with the targeted probabilities almost entirely determining the number of incorrect decisions. After the switch of the pointing toward Dimorphos, the test adjusted the decision mode to utilize the information about

which filter was no longer performing updates due to physically inconsistent measurements. No false alarm occurred in this mode, suggesting that the chosen tuning might be appropriate.

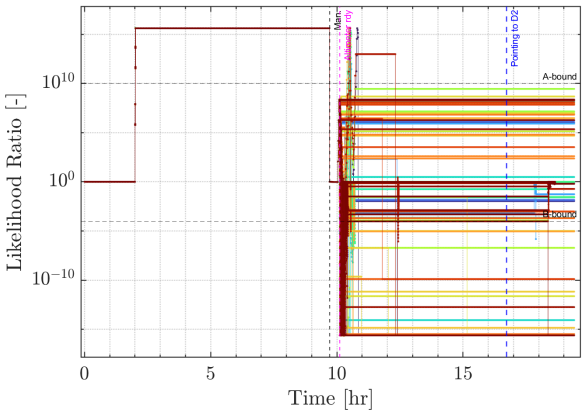

Figure 5: Evolution over time of the Innovations Likelihood ratio - Unsafe EXP.

The unsafe scenario results showed that the ratio (fig. 5) quickly moved toward accepting the H_1 hypothesis for most samples after the manoeuvre, with only 8 m.d. occurrences in 42510 taken decisions. Nevertheless, it is significant that multiple resets occurred in a short time frame and all led to the same correct evaluation. The secondary mode similarly managed to detect the safety risk. However, the threshold of $1\,hr$ appeared to be excessively long as several samples did not exceed it in time to avoid the collision after the last restart. The results confirmed that the test was more prone to produce a conservative decision leaning toward f.a. rather than m.d., as desired.

4. Highlights and conclusions

The development of an autonomous failure detection system focused on Navigation functionalities was tackled, with no identified method simpler and more cost-effective than an accurate and robust navigation filter. In the Hera mission scenario, the MOCRE showed limitations in accuracy, particularly in filtering out measurement noise and the other error sources. The second proposed approach aimed at providing an independent and robust safety assessment while reducing computational demand compared to the navigation filter, but fell short due to the sensitivity of velocity estimation errors to the uncorrected error sources. The hypothesis testing framework, conceived as an independent check of the navigation solution rather than a completely independent system, achieved promising outcomes. However, further testing would be needed to better characterize its reliability. Overall, the study indicated that algorithms for detecting hazardous trajectory failures can be designed to offer some degree of accuracy. However, the demand for complete independence in the assessment appears too strict, given the limitations in on-board computer resources and measurements acquisition. Future work should explore methods to account for the presence of the secondary body avoiding the necessity of a restrictive "Keep-out Sphere" approach. However, the author perceives limited room for resolving the challenge solely from a Navigation standpoint.

5. Acknowledgements

This research was carried out during an internship on the Hera Mission GNC at ESA ESTEC. Thanks to my supervisors Jesús Gil-Fernández and Diego Escorial Olmos for the opportunity, and to the entire Hera mission team for their support.

References

[1] J. Russell Carpenter and F. Landis Markley. Sequential Wald Test Employing a Constrained Filter Bank: Application to Spacecraft Conjunctions. *J Optim Theory Appl*, 191(2):440–458, December 2021.

[2] Michel Patrick et al. The ESA Hera Mission: Detailed Characterization of the DART Impact Outcome and of the Binary Asteroid (65803) Didymos. *Planet. Sci. J.*, 3(7), July 2022.

[3] Williams B. et al. OSIRIS-REx Flight Dynamics and Navigation Design. *Space Science Reviews*, 214(4):69, June 2018.

[4] Jeroen L. Geeraert and Jay W. McMahon. Square-Root Unscented Schmidt–Kalman Filter. *Journal of Guidance, Control, and Dynamics*, 41(1):280–287, January 2018.

[5] Dan Simon. *Optimal state estimation: Kalman, H infinity, and nonlinear approaches*. John Wiley & Sons, 2006.